

Finite-Temperature Wigner Phase-Space Sampling and Temperature Effects on the Excited-State Dynamics of 2-Nitronaphthalene

J. Patrick Zobel,^{*} Juan J. Nogueira,^{*} and Leticia González^{*}

*Institute of Theoretical Chemistry, University of Vienna, Währinger Straße 17, A-1090
Vienna, Austria*

E-mail: patrick.zobel@univie.ac.at; nogueira.perez.juanjose@univie.ac.at;
leticia.gonzalez@univie.ac.at

Electronic Supplementary Information

In Section S1, we present a description on how to perform Wigner phase-space sampling according to eq. (5) in the main paper. In Section S2, we present a discussion of the finite-temperature effects in vibrational sampling and excited-state dynamics. In Section S3, we present a description of the excited-states computed at the minimum-energy Franck-Condon geometry.

S1 Wigner Phase-Space Sampling

The Wigner function can be used for phase-space sampling. This is, for example, necessary in order to generate initial nuclear coordinates and momenta prior to perform non-adiabatic molecular dynamics simulations. To this purpose, we can choose a random pair of coordinates and momenta (p_i, q_i) , calculate its (quasi-)probability $W(p_i, q_i)$, and compare it with a random number k from a uniform distribution of $k \in [0, 1]$. If $W(p_i, q_i) \geq k$, we accept the coordinates and momenta (p_i, q_i) for our sample while if $W(p_i, q_i) < k$, we discard (p_i, q_i) and choose a new pair (p_j, q_j) . If $W(p_i, q_i) < 0$, i.e., the Wigner function W has a negative value for (p_i, q_i) , we always discard (p_i, q_i) in line with the interpretation that coordinates for which W is negative are unaccessible in experiment.¹⁻³

The Wigner function is a functional of the wave function, i.e., $W = W[\Psi]$, as is evident from eq. (1) in the main paper. Similar to the problem of the unattainable exact electronic wave function in electron-structure theory, also when sampling the nuclear phase space of a molecule, one generally does not know the exact nuclear wave function, calling for the use of some approximate description of the nuclear motion. A common simple approximation is to describe the (non-linear) N -atomic molecule as a system of $3N - 6$ uncoupled one-dimensional harmonic oscillators.⁴ Then, by using the product wave function $\Psi(\mathbf{q}) = \prod_{i=1}^{3N-6} \varphi(q_i)$ composed of the eigenfunctions $\varphi(q_i)$ of the one-dimensional harmonic oscillators of normal modes i , the Wigner function factorizes as

$$W[\Psi](\mathbf{q}, \mathbf{p}) = \prod_{i=1}^{3N-6} W[\varphi(q_i)](q_i, p_i) = \prod_{i=1}^{3N-6} W_i \quad (1)$$

The eigenfunctions of the harmonic oscillator are known analytically and read for the normal mode i in the vibrational state n

$$\varphi_n(q_i) = \frac{1}{\sqrt{2^n n!}} \left(\frac{\mu_i \omega_i}{\pi \hbar} \right)^{1/4} \exp\left(-\frac{\mu_i \omega_i^2 q_i^2}{2\hbar}\right) H_n\left(\sqrt{\frac{\mu_i \omega_i}{\hbar}} q_i\right) \quad (2)$$

where ω_i and μ_i are the frequencies and reduced masses, respectively, and H_n is the n -th order Hermite polynomial. Thus, one only needs to calculate ω_i and μ_i for the uncoupled harmonic oscillators (normal modes) to obtain an expression for the Wigner function W . More specifically, the Wigner functions of the harmonic oscillator read

$$W_i[\varphi_n](q_i, p_i) = \frac{1}{\pi\hbar} (-1)^n \exp\left(-\frac{2H_i}{\hbar\omega_i}\right) L_n\left(\frac{4H_i}{\hbar\omega_i}\right) \quad (3)$$

where $L_n(x)$ is the n -th order Laguerre polynomial, and $H_i = p_i^2/2\mu_i + 1/2\mu_i\omega_i^2 q_i^2$ is the classical Hamiltonian of the harmonic oscillator. If one considers the uncoupled harmonic oscillators to be in their ground state $\varphi_0(q_i)$, the one-dimensional Wigner functions W_i read simply

$$W_i[\varphi_0](q_i, p_i) = \frac{1}{\pi\hbar} \exp\left(-\frac{p_i^2/\mu_i + \mu_i\omega_i^2 q_i^2}{\hbar\omega_i}\right) \quad (4)$$

Restricting the system to always be in the ground state bears both advantage and disadvantage. As is apparent $W_i[\varphi_0] \geq 0 \quad \forall (q_i, p_i)$, i.e., the Wigner function is either positive or zero for the system in the ground state, and one, thus, does not need to deal with the situation of negative (quasi-)probabilities. However, restricting the system to always be in the ground state corresponds to the hypothetical situation of the system at zero temperature ($T = 0$ K). Certainly, a more realistic description of the system taking into account finite temperature is desired.

Temperature may be defined as the thermodynamic quantity that, multiplied by the Boltzmann constant k_B , equals the energy per degree of freedom that is available to promote the system from its ground to its excited states.⁵ Thus, temperature is not a straight measure of the energy of a system; this situation only refers to the special case where the energy of the ground state of the system equals zero. This case, however, is not met when describing the vibrational motion of a molecule, where the ground state is already at an elevated energy, the zero-point energy (ZPE). At finite temperature,

both ground and excited vibrational states possess non-zero population.

The probability $P_n(T)$ to populate the state n with energy E_n in a canonical ensemble can be computed by a Boltzmann distribution

$$P_n(T) = \frac{\exp\left(-\frac{E_n}{k_B T}\right)}{\sum_n \exp\left(-\frac{E_n}{k_B T}\right)} = \frac{\exp\left(-\frac{E_n}{k_B T}\right)}{Z(T)} \quad (5)$$

where $Z(T)$ is the canonical partition function. For the harmonic oscillator with energy levels

$$E_n = \hbar\omega(n + 1/2) \quad \text{where } n = 0, 1, 2, \dots \quad (6)$$

there exists a closed-form expression for $Z(T)$ reading

$$Z(T) = \sum_{n=0}^{\infty} \exp\left(-\frac{\hbar\omega}{k_B T}(n + 1/2)\right) = \frac{\exp\left(-\frac{\hbar\omega}{2k_B T}\right)}{1 - \exp\left(-\frac{\hbar\omega}{k_B T}\right)} \quad (7)$$

The temperature-dependent energy of the harmonic oscillator in the canonical ensemble is then given by

$$E(T) = \sum_{n=0}^{\infty} P_n(T) E_n = \frac{\hbar\omega}{2} + \hbar\omega \frac{\exp\left(-\frac{\hbar\omega}{k_B T}\right)}{1 - \exp\left(-\frac{\hbar\omega}{k_B T}\right)} = \text{ZPE} + \varepsilon(T) \quad (8)$$

i.e., it is the sum of the temperature-independent ZPE and a thermal-energy contribution $\varepsilon(T)$. For $\hbar\omega/k_B T \approx 0$, a first-order Taylor expansion of the thermal energy yields $\varepsilon(T) = k_B T - \hbar\omega$. Thus, in the high-temperature (or low-frequency) limit we find that approximately

$$\lim_{k_B T \gg \hbar\omega} E(T) \approx k_B T \quad (9)$$

Using the temperature-dependent probabilities $P_n(T)$ from eq. (5), we can now perform Finite-Temperature Wigner Phase-Space (FITWIPS) sampling. In practice, for phase-space sampling, for each normal mode i , we proceed as follows:

1. We determine the probabilities to populate each vibrational state at a given temperature using eq. (5).
2. Following these probabilities, we stochastically select a vibrational state, say φ_n , which determines the Wigner function $W[\varphi_n]$.
3. We then select random coordinates and momenta (q_i, p_i) , and calculate the value of the Wigner function corresponding to our chosen state, i.e., $W[\varphi_n](q_i, p_i)$, using eq. (3).
4. We compare $W[\varphi_n](q_i, p_i)$ against a random number $k \in [0, 1]$. If $W[\varphi_n](q_i, p_i) \geq k$, we accept (q_i, p_i) for our sample, otherwise we discard (q_i, p_i) and start again at step 2.

We point out again that $W[\varphi_n](q_i, p_i)$ can be negative for $n \geq 1$, in which case we always discard (q_i, p_i) , as discussed above.

S2 Finite-Temperature Effects

Having introduced the concept of FITWIPS sampling in the previous section, in this section we discuss for pedagogical purposes the effects that a finite temperature can have in phase-space sampling of simple molecules. Specifically, we first compare the ZPE and thermal-energy contributions to the total vibrational energy for a range of molecules and motivate possible effects that the population of vibrationally excited levels can have on the excited-state dynamics of molecules.

S2.1 ZPE and Thermal-Energy Contributions

For a normal mode with frequency ω , the probabilities P_n to populate ground and excited states depend on the quotient ω/T [see eqs. (5) and (7)]. For high-frequency

modes ($\omega \gg T$), the system will populate primarily the ground state, while for low-frequency modes ($\omega \ll T$), the population will be spread over a number of states. We show this exemplarily in Figure S1, where, e.g., for $T = 300$ K and $\omega = 1000$ cm^{-1} all population is in the ground state. At the same temperature, for $\omega = 500$ cm^{-1} already 8 % of the population is in the first excited state. And for $\omega = 100$ cm^{-1} , P_0 is only 38 % and all states up to $n = 7$ have contributions of $P_n > 1$ %. At higher temperatures, the population of the vibrationally excited states naturally grows. For example, at $T = 500$ K, the population of all excited vibrational states sums up to $\sum_{n \geq 1} P_n = 24$ % and 75 % for $\omega = 500$ cm^{-1} and 100 cm^{-1} , respectively.

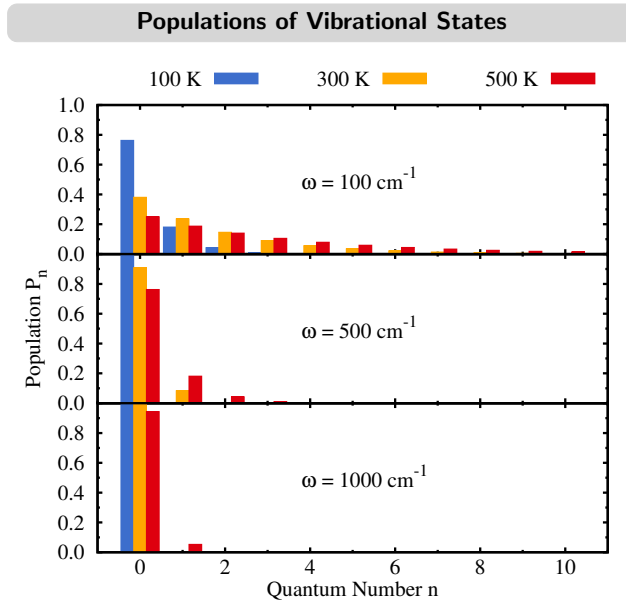


Figure S1: Temperature-dependent population of the states of harmonic oscillators with different frequencies ω .

When we calculate the total energy in a vibrational mode according to eq. (8), we will have different contributions of the (temperature-independent) ZPE and the thermal-energy contribution that is due to the population of vibrationally excited states. For a high-frequency mode, the thermal-energy contribution is very small as the excited-state populations are negligible and the total energy is in a good approximation given by the ZPE. In contrast, for a low-frequency mode, the situation is reversed and

the thermal-energy contribution can be much larger than the ZPE (see Figure S2). These cases are illustrated in Table S1, where the ZPE and thermal-energy contributions of all normal modes of formamide and ethene for a temperature of $T = 300$ K are tabulated.

Table S1: Contribution of ZPE and thermal energy $\epsilon(T)$ to the total energy $E(T)$ in cm^{-1} of the normal modes of formamide and ethene at $T = 300$ K. Normal modes calculated at MP2/6-31G* level of theory using Gaussian09.⁶

Mode	Formamide				Ethene			
	ω_i	ZPE _{<i>i</i>}	$\epsilon_i(T)$	$E_i(T)$	ω_i	ZPE _{<i>i</i>}	$\epsilon_i(T)$	$E_i(T)$
ω_1	132.08	66.04	149.38	215.42	845.58	422.79	14.90	437.69
ω_2	564.96	282.48	40.28	322.76	938.04	469.02	10.54	479.56
ω_3	649.30	324.65	30.17	354.82	992.50	496.25	8.57	504.82
ω_4	1058.31	529.15	6.65	535.80	1089.30	544.65	5.89	550.54
ω_5	1074.72	537.36	6.24	543.60	1266.11	633.05	2.92	635.98
ω_6	1305.22	652.61	2.49	655.10	1412.52	706.26	1.61	707.87
ω_7	1458.89	729.44	1.33	730.78	1522.56	761.28	1.02	762.30
ω_8	1657.87	828.93	0.58	829.51	1726.75	863.37	0.43	863.81
ω_9	1841.38	920.69	0.26	920.95	3238.21	1619.10	0.00	1619.10
ω_{10}	3066.37	1533.18	0.00	1533.18	3256.05	1628.02	0.00	1628.02
ω_{11}	3689.79	1844.89	0.00	1844.89	3332.88	1666.43	0.00	1666.44
ω_{12}	3843.70	1921.85	0.00	1921.85	3356.10	1678.05	0.00	1678.05
Total		10171.29	237.43	10408.72		11488.30	45.93	11534.23
C [%]		97.72	2.28	100.00		99.60	0.40	100.00

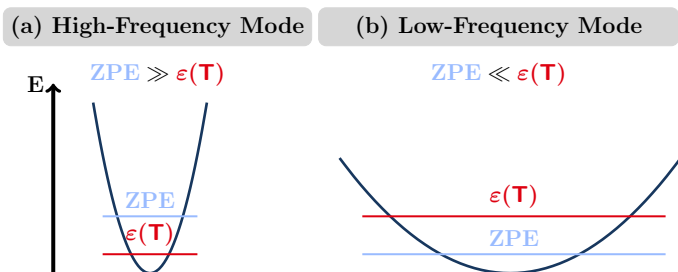


Figure S2: Comparison of zero-point and thermal-energy contributions for high- and low-frequency normal modes.

When looking at the lowest-frequency normal mode of formamide ($\omega_1 = 132 \text{ cm}^{-1}$), we find that the thermal-energy contribution is much larger than the ZPE, i.e., $\epsilon_1(T) =$

2.2 ZPE₁. In contrast, for the higher-frequency normal modes, ZPE_{*i*} is always larger than $\varepsilon_i(T)$, and $\varepsilon_i(T) < 1\%$ of the total energy for modes $n \geq 6$. Considering all normal modes of formamide, the ZPE and thermal contribution amount to 10171 and 237 cm⁻¹, respectively, corresponding to a percentage contribution of $C = 97.7\%$ and $C = 2.3\%$ of the total vibrational energy. When we now compare the results of formamide with the results for ethene –two molecules with the same number of atoms, i.e., same number of normal modes –we see that the thermal-energy contribution is much smaller for ethene ($C = 0.4\%$) than for formamide ($C = 2.3\%$). This is due to the, in average, larger frequencies of the normal modes of ethene; especially, the lowest-frequency normal mode $\omega_1 = 845\text{ cm}^{-1}$ contributes only 15 cm⁻¹ to the thermal energy $\varepsilon_1(T = 300\text{ K})$, while the lowest-frequency normal mode $\omega_1 = 132\text{ cm}^{-1}$ of formamide contributes $\varepsilon_1(T = 300\text{ K}) = 150\text{ cm}^{-1}$ –the ten-fold amount of $\varepsilon(T)$.

As the comparison of formamide and ethene has illustrated, the thermal-energy contribution is unique for every molecule: it depends on the distribution of the normal-mode frequencies of the system. If the system 1 possesses more low-frequency modes than system 2, then its thermal-energy contribution to the total energy will be larger than that of system 2, and, thus, inclusion of finite-temperature effects will be more important for the description of system 1 than for system 2. Typically, one associates high-frequency normal modes with very rigid internal movements of the molecule, i.e., when atoms in a molecule are bound by strong chemical bonds, the normal modes describing the vibrations between these atoms possess rather high frequencies. In contrast, normal modes describing the vibration of loosely-bound atoms –as found, e.g., in van-der-Waals clusters or systems exhibiting hydrogen bonding –possess rather low frequencies. Additionally, low frequencies are found for torsional motion in molecules, e.g., that of methyl groups in organic molecules. In terms of chemical structure, we can, thus, propose that the less rigid is the structure of a molecule, the larger the contribution of the thermal energy $\varepsilon(T)$ to the total energy $E(T)$ will be.

To awake awareness on the importance of the thermal energy, we now investi-

gate its size for a sample of molecules, for instance using the Thiel’s benchmark set,⁷ which comprises 28 small and medium-sized organic chromophores (see Table S2). For each molecule, we performed a geometry optimization and frequency calculation at the second-order Møller-Plesset perturbation theory (MP2)⁸ using the 6-31G* basis set⁹ as implemented in the Gaussian09 program package.⁶ As input geometries, we employed the MP2/6-31G*-optimized geometries reported in Ref. 7, which in the cases of formamide, acetamide, propanamide, naphthalene, adenine, and cytosine represented transition states, i.e., conformations with one imaginary-frequency normal mode. Re-optimization of all molecules at this level of theory lead to energetic minima, with the exception of naphthalene. For naphthalene, re-optimization consistently lead to a planar structure exhibiting one imaginary-frequency normal mode with $\omega = 238i \text{ cm}^{-1}$ –at the MP2/6-31G*level of theory using Gaussian09 – and we, thus, excluded naphthalene from our analysis. Note that this predicted nonplanarity appears to be a common problem for certain combinations of correlated electronic structure methods and basis sets for arenes.¹⁰ For all other molecules, we present the ZPE, thermal-energy contribution $\varepsilon(T)$, and total energy $E(T)$ for a temperature of $T = 300 \text{ K}$ in Table S2.

As can be seen in Table S2, the contribution of the thermal energy $\varepsilon(T)$ to the total energy $E(T)$ ranges from 0.12 % (formaldehyde) to 4.26 % (thymine). As expected, we find the largest thermal-energy contribution for the molecules with non-rigid structural elements such as CH_3 or NH_2 groups, e.g., in nucleobases or amides. The molecules in Thiel’s benchmark set either are cyclic or possess one or more double bonds which hinders low-frequency motions such as torsion. Thus, these molecules possess rather rigid structures, and the typical size of the thermal-energy contribution found here is much smaller than the size of $\varepsilon(T)$ for other classes of molecules with more flexible structure.

Table S2: ZPE, thermal energy $\varepsilon(T)$, and total energy $E(T)$ in eV as well as percentage of contributions $C(\text{ZPE})$ and $C(\varepsilon)$ of the ZPE and thermal energy, respectively, for the molecules contained in the Thiel benchmark set⁷ as well as 2-nitronaphthalene and $\text{Ru}(\text{bpy})_3^{2+}$ at a temperature of $T = 300$ K. Frequencies calculated at MP2/6-31G* level of theory using Gaussian09.

Molecule	ZPE	$\varepsilon(T)$	$E(T)$	$C(\text{ZPE})$	$C(\varepsilon)$
Acetamide	2.054	0.063	2.117	97.01	2.98
Acetone	2.342	0.070	2.413	97.08	2.91
Adenine	3.089	0.121	3.210	96.23	3.76
Benzene	2.754	0.048	2.802	98.26	1.73
Benzoquinone	2.315	0.100	2.416	95.82	4.17
Butadiene	2.362	0.051	2.413	97.87	2.12
Cyclopentadiene	2.565	0.037	2.602	98.56	1.43
Cyclopropene	1.566	0.013	1.579	99.14	0.85
Cytosine	2.725	0.104	2.829	96.32	3.67
Ethene	1.424	0.005	1.430	99.60	0.39
Formaldehyde	0.745	0.001	0.746	99.87	0.12
Formamide	1.261	0.029	1.290	97.71	2.28
Furan	1.928	0.026	1.954	98.66	1.33
Hexatriene	3.284	0.110	3.394	96.75	3.24
Imidazole	1.966	0.026	1.992	98.67	1.32
Norbornadiene	3.571	0.054	3.625	98.49	1.50
Octatetraene	4.204	0.170	4.375	96.09	3.90
Propanamide	2.863	0.093	2.957	96.84	3.15
Pyrazine	2.120	0.038	2.158	98.23	1.76
Pyridazine	2.093	0.040	2.134	98.08	1.91
Pyridine	2.445	0.041	2.487	98.31	1.68
Pyrimidine	2.126	0.038	2.164	98.23	1.76
Pyrrole	2.277	0.033	2.310	98.53	1.46
Tetrazine	1.412	0.038	1.450	97.35	2.64
Thymine	3.180	0.141	3.321	95.73	4.26
Triazine	1.804	0.035	1.839	98.08	1.91
Uracil	2.398	0.095	2.494	96.17	3.82
2-Nitronaphthalene	4.075	0.177	4.253	95.82	4.18
$\text{Ru}(\text{bpy})_3^{2+}$	12.771	0.730	13.501	94.59	5.41

S2.2 Potential Effects on Excited-State Dynamics

When one adds the thermal energy $\varepsilon(T)$ to the ZPE, the system naturally possesses more vibrational energy. As can be seen in Table S1, this increase in energy can be up to 0.2 eV for the small and medium-sized organic molecules in Thiel’s benchmark set at a temperature of $T = 300$ K. The increase can become larger when one considers larger systems with a larger number of low-frequency normal modes amounting to, e.g., $\varepsilon(T = 300\text{ K}) = 0.7$ eV for the metal complex $\text{Ru}(\text{bpy})_3^{2+}$ (recall Table S2).

Although an additional 0.1 eV (2.3 kcal/mol) vibrational energy may appear rather small, already this amount of additional energy might have affect excited state dynamics. As an illustration, consider a hypothetical system with two electronic states as in Figure S3a: after excitation, the system could climb the potential-energy barrier and undergo some further reaction or get trapped in the excited state minimum and relax to the ground state via fluorescence. Using transition state theory one can estimate a rate constant k_R for the reaction in the excited state, where the potential energy barrier ΔE serves as the activation energy E_A

$$k_R = \frac{k_B T}{h} \exp\left(-\frac{E_A}{k_B T}\right) \quad (10)$$

For fluorescence, one typically¹¹ finds room-temperature rates of $k_F = 10^6$ - 10^9 s⁻¹. Thus, the excited-state reaction can compete with fluorescence if its rate constant k_R is similar or larger that that of fluorescence. Using $k_R = k_F = 10^6$ - 10^9 s⁻¹ and eq. (10) we find that the reaction occurs if its barrier is $\Delta E < 0.22$ - 0.40 eV. Therefore, if one includes the thermal-energy contribution $\varepsilon(T)$ in the description of the system, this additional energy can significantly alter the kinetics of the reaction by effectively reducing the required activation energy for the excited-state reaction E_A . The rate of

the reaction is then increased by a factor of

$$\frac{k'_R}{k_R} = \frac{\exp\left(\frac{-(E_A - \varepsilon(T))}{RT}\right)}{\exp\left(\frac{-E_A}{RT}\right)} = \exp\left(\frac{\varepsilon(T)}{RT}\right) \quad (11)$$

which is, e.g., $k'_R/k_R \approx 50$ if $\varepsilon(T) = 0.1$ eV at $T = 300$ K. Note, that this is a simplified model that assumes an isolated system whose thermal-energy contribution is not transferred to the environment and it is completely accumulated in the reaction coordinate of the excited-state reaction.

Finite temperatures can also influence the excited-state dynamics in a different manner. As illustrated in Figure S3b, at higher temperatures, the system occupies more geometries displaced further from the minimum-energy geometry than at lower temperatures. This follows from the fact that at higher temperatures the systems populates higher vibrational states, more extended than the vibrational ground state. Further, the maximum of the distribution gradually shifts from the minimum of the potential energy (ground state of the harmonic oscillator) to the reflection points of the potential (excited states of the harmonic oscillator). Thus, at higher temperatures one can populate more strongly displaced geometries that can lie closer to the maxima of the potential-energy barriers in the excited state. Then, the system requires less energy to overcome these barriers which can open up new reaction paths.

S2.3 Potential Pitfalls of FITWIPS

When extending (standard) zero-temperature Wigner sampling to FITWIPS, one accounts for the finite temperature by allowing the population of vibrationally excited states. In general, this allows for a more realistic phase-space sampling as one is not restricted to the idealized zero-temperature situation. One can run into problems, however, when using the harmonic-oscillator approximation in FITWIPS in the case of high temperatures and low frequencies, as then, highly excited vibrational states

can be populated. For example, as was shown in Figure S1, for $\omega = 100 \text{ cm}^{-1}$ and $T = 500 \text{ K}$, vibrational states with quantum numbers up to $n = 11$ are populated by about $P_n > 1 \%$. For these highly excited states, anharmonicity can become more important. In the worst case, one could even populate one of the (infinitely many) harmonic oscillator bound states that lies above the dissociation limit of the real (anharmonic) potential.

Circumventing these problems is not an easy task as the only straightforward approach consists in first computing the real potential energy surfaces (PES) and calculate the real vibrational eigenstates considering anharmonicity and a finite number of bound states, before performing the phase-space sampling. Unfortunately, the immense computational cost associated to the calculation of the PES prohibits this approach for all but the smallest systems. A complementary approach able to capture (at least part of) the anharmonicity of the potential is to employ (ab initio) molecular dynamics simulations to explore the PES. In this case, the system possess an energy of $k_B T$ in each degree of freedom corresponding to the high-temperature limit of the vibrational energy [eq. (9)]. This yields a better description of low-frequency modes where the largest contribution of the vibrational energy is given by thermal energy contribution compared to zero-temperature Wigner sampling; however, for all higher-frequency modes one misses the ZPE completely. As the ZPE is at least for moderate temperatures –say, 300 K –often larger than $k_B T$, the largest part of the total energy is not accounted for. Additionally, with the smaller energy available in classical sampling, one then is able to sample only a very narrow region with low energies around the energetic minimum of these high-frequency normal modes. Finally, one should stress out, that the high-temperature limit energy of $k_B T$ in classical sampling does not represent the thermal energy contribution $\varepsilon(T)$ in quantum sampling. In fact, usually $\varepsilon(T) \ll k_B T$. We then conclude that no affordable conformational sampling method is able to correctly describe the real PES, and provide the correct energy, so that in practical applications, one should decide for each system individually which sampling

method is most suitable.

In the main paper, we present excited-state dynamics simulations of the organic chromophore 2-nitronaphthalene (2NN). As is shown, it is mandatory that the molecule is given the correct energy so that the nuclear motion is simulated adequately. Given only the small thermal-energy contribution available, e.g., from molecular dynamics simulations, the motion of the molecule would be too slow and it would possess little energy to climb energy barriers in the excited states. It is therefore advisable to use Wigner phase-space sampling to include at least the ZPE (at zero temperature) –that accounts for, e.g., 96 % of the total vibrational energy at a temperature of $T = 300$ K –or both the ZPE and thermal-energy contributions (using FITWIPS).

For 2NN, the lowest-frequency normal mode corresponds to the nitro-group torsion with a frequency of $\omega = 87 \text{ cm}^{-1}$. For this frequency, Figure S4 shows the coordinate probability distributions of the Wigner ensembles at temperatures of 0, 300, and 500 K, as well as those of the harmonic oscillator eigenstates $n = 0, 8,$ and 12 . The eigenstates $n = 8$ and $n = 12$ are the highest excited eigenstates with a thermal population $P_n \geq 1 \%$ at $T = 300$ and 500 K, respectively. As it can be expected, the probability distributions of the vibrational ground state ($n = 0$) differs considerable from that of the excited modes for $n = 8, 12$ (Figure S4a). These differences translate to the thermally averaged probability distributions for the finite temperatures ($T = 300, 500$ K), see Figure S4(b), as these distributions do not possess their maximum at $x = 0$ anymore, as the zero-temperature case does, where x is the normal-coordinate displacement with respect to the minimum-energy geometry. Instead, these distributions display two maxima located symmetrically at positive and negative displacements of $|x| \sim 0.6$ and long tails that extend 2-3 times further than the zero-temperature distribution. These effects can influence notably the excited state dynamics at different temperatures as is shown for 2NN in the main manuscript.

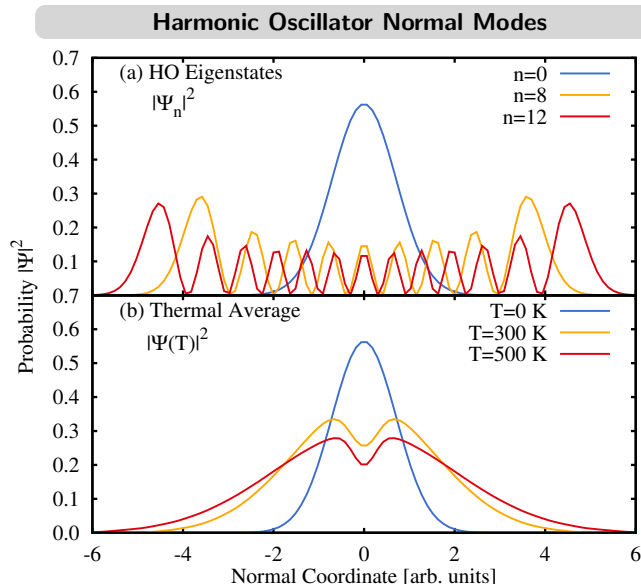


Figure S4: (a) Normal mode probability distributions $|\Psi_n|^2$ for eigenfunctions of the harmonic oscillator. (b) Thermal average of probability distributions $|\Psi(T)| = \sum_i P_i(T) |\Psi_i|^2$ for different temperatures. Probabilities $P_i(T)$ determined for frequency $\omega = 87 \text{ cm}^{-1}$ of the nitro group torsional mode of 2NN.

S3 Excited States at the Franck-Condon Geometry

Here, we present a characterization of the excited states of 2NN computed at the minimum-energy Franck-Condon geometry in Figure S5. The geometry optimization as well as the calculation of the excited states was conducted at the PBE0/DZP level of theory using ADF2016.¹² The natural transition orbitals (NTOs) shown in Figure S5 possess weights of at least 98 %, thus, describing the individual excited states sufficiently. The excited states are characterized as by the shape of their main NTOs ($n\pi^*$ vs. $\pi\pi^*$) and classified either as charge-transfer (CT) or localized excitations (LE).

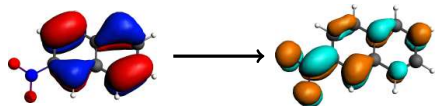
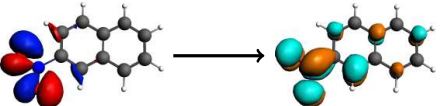
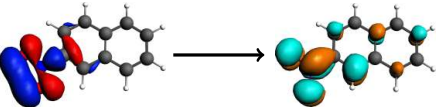
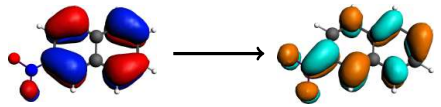
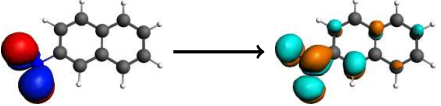
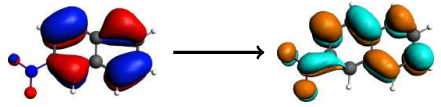
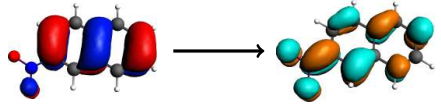
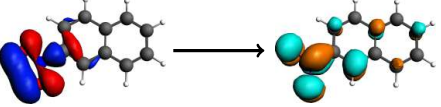
State	Energy (eV)	f_{osc}	Character	Natural Transition Orbitals
S_1	3.80	0.064	$S_{CT}(\pi\pi^*)$	
S_2	3.85	0.000	$S_{LE}(n\pi^*)$	
S_3	4.47	0.100	$S_{LE}(\pi\pi^*)$	
S_4	4.50	0.000	$S_{LE}(n\pi^*)$	
T_1	2.85	0.000	$T_{CT}(\pi\pi^*)$	
T_2	3.32	0.000	$T_{LE}(n\pi^*)$	
T_3	3.32	0.000	$T_{LE}(\pi\pi^*)$	
T_4	3.67	0.000	$T_{LE}(\pi\pi^*)$	
T_5	3.77	0.000	$T_{CT}(\pi\pi^*)$	
T_6	4.00	0.000	$T_{LE}(n\pi^*)$	

Figure S5: Excited states computed at the Franck-Condon geometry. f_{osc} denotes the oscillator strength.

References

- (1) Feynman, R. P. Simulating Physics with Computers. *Int. J. Theor. Phys.* **1982**, *21*, 467–488.
- (2) Feynman, R. P. In *Quantum Implications: Essays in Honour of David Bohm*; Hiley, B. J., Peat, F. D., Eds.; Routledge & Kegan Paul Ltd., 1987; Chapter 13.
- (3) Leibfried, D.; Pfau, T.; Monroe, C. Shadows and Mirrors: Reconstructing Quantum States of Atom Motion. *Physics Today* **1998**, *51*, 22–28.
- (4) Sun, L.; Hase, W. L. Comparison of classical and Wigner sampling of transition state energy level for quasiclassical trajectory chemical dynamics simulations. *J. Chem. Phys.* **2010**, *133*, 044313.
- (5) Fließbach, T. *Statistische Physik*, 5th ed.; Spektrum Akademischer Verlag, 2010.
- (6) Frisch, M. J.; Trucks, G. W.; Schlegel, H. B.; Scuseria, G. E.; Robb, M. A.; Cheeseman, J. R.; Scalmani, G.; Barone, V.; Mennucci, B.; Petersson, G. A.; Nakatsuji, H.; Caricato, M.; Li, X.; Hratchian, H. P.; Izmaylov, A. F.; Bloino, J.; Zheng, G.; Sonnenberg, J. L.; Hada, M.; Ehara, M.; Toyota, K.; Fukuda, R.; Hasegawa, J.; Ishida, M.; Nakajima, T.; Honda, Y.; Kitao, O.; Nakai, H.; Vreven, T.; Montgomery Jr., J. A.; Peralta, J. E.; Ogliaro, F.; Bearpark, M.; Heyd, J. J.; Brothers, E.; Kudin, K. N.; Staroverov, V. N.; Kobayashi, R.; Normand, J.; Raghavachari, K.; Rendell, A.; Burant, J. C.; Iyengar, S. S.; Tomasi, J.; Cossi, M.; Rega, N.; Millam, J. M.; Klene, M.; Knox, J. E.; Cross, J. B.; Bakken, V.; Adamo, C.; Jaramillo, J.; Gomperts, R.; Stratmann, R. E.; Yazyev, O.; Austin, A. J.; Cammi, R.; Pomelli, C.; Ochterski, J. W.; Martin, R. L.; Morokuma, K.; Zakrzewski, V. G.; Voth, G. A.; Salvador, P.; Dannenberg, J. J.; Dapprich, S.; Daniels, A. D.; Farkas, Ö.; Foresman, J. B.; Or-

- tiz, J. V.; Cioslowski, J.; Fox, D. J. Gaussian 09, Revision E.01, Gaussian, Inc., Wallingford CT. 2009.
- (7) Schreiber, M.; Silva-Junior, M. R.; Sauer, S. P. A.; Thiel, W. Benchmarks for electronically excited states: CASPT2, CC2, CCSD, and CC3. *J. Chem. Phys.*, **2008**, *128*, 134110.
- (8) Frisch, M. J.; Head-Gordon, M.; Pople, J. A. A direct MP2 gradient method. *Chem. Phys. Lett.* **1990**, *166*, 275–280.
- (9) Hehre, W. J.; Ditchfield, R.; Pople, J. A. Self-Consistent Molecular Orbital Methods. XII. Further Extensions of Gaussian-type Basis Sets for Use in Molecular Orbital Studies of Organic Molecules. *J. Chem. Phys.* **1972**, *56*, 2257–2261.
- (10) Moran, D.; Simmonett, A. C.; Leach III, F. E.; Allen, W. D.; R., S. P. V.; Schaefer III, H. F. Popular Theoretical Methods Predict Benzene and Arenes To Be Nonplanar. *J. Am. Chem. Soc.* **2006**, *128*, 9342–9343.
- (11) El-Sayed, M. A. The Triplet State: Its Radiative and Nonradiative Properties. *Acc. Chem. Res.* **1968**, *1*, 8–16.
- (12) Baerends, E. J.; Ziegler, T.; Atkins, A. J.; Autschbach, J.; Bashford, D.; Bérces, A.; Bickelhaupt, F. M.; Bo, C.; Boerrigter, P. M.; Cavallo, L.; Chong, D. P.; Chulhai, D. V.; Deng, L.; Dickson, R. M.; Dieterich, J. M.; Ellis, D. E.; van Faassen, M.; Fan, L.; Fischer, T. H.; Fonseca Guerra, C.; Franchini, M.; Ghysels, A.; Giammona, A.; van Gisbergen, S. J. A.; Götz, A. W.; Groeneveld, J. A.; Gritsenko, O. V.; Grüning, M.; Gusarov, M. S.; Harris, F.; van den Hoek, P.; Jacob, C.; Jacobsen, H.; Jensen, L.; Kaminski, J. W.; van Kessel, G.; Kootstra, F.; Kovalenko, A.; Krykunov, M. V.; van Lenthe, E.; McCormack, D. A.; Michalak, A.; Mitoraj, M.; Morton, S. M.; Neugebauer, J.; Nicu, V. P.; Noodleman, L.; Osinga, V. P.; Patchkovskii, S.; Pavanello, M.;

Peeples, C. A.; Philipsen, P. H. T.; Post, D.; Pye, C. C.; Ravenek, W.; Rodríguez, J. I.; Ros, P.; Rüger, R.; Schipper, P. R. T.; van Schoot, H.; Schreckenbach, G.; Seldenthuis, J. S.; Seth, M.; Snijders, J. G.; Solà, M.; Swart, M.; Swerhone, D.; te Velde, G.; Vernooijs, P.; Versluis, L.; Visscher, L.; Visser, O.; Wang, F.; Wesolowski, T. A.; van Wezenbeek, E. M.; Wiesenekker, G.; Wolff, S. K. .; Woo, T. K.; Yakovlev, A. L. ADF2016, SCM, Theoretical Chemistry, Vrije Universiteit, Amsterdam, The Netherlands, <http://www.scm.com>. 2016.